Applied Clay Science 146 (2017) 380–387

Contents lists available at ScienceDirect

Applied Clay Science

journal homepage: www.elsevier.com/locate/clay

Research paper

Ceramic behavior of ball clay with gadolinium oxide (Gd_2O_3) addition

M.F. Hernández[a,b,*], M.S. Conconi[a], M. Cipollone[b,c], M.S. Herrera[a], N.M. Rendtorff[a,b]

[a] Centro de Tecnología de Recursos Minerales y Cerámica (CETMIC): (CIC-CONICET-CCT La Plata), Camino Centenario y 506 s/n, C.C.49 (B1897ZCA), M.B. Gonnet, Argentina
[b] Dpto. De Química, Facultad de Ciencias Exactas, Universidad Nacional de La Plata, UNLP, 47 y 115 s/n, La Plata, Argentina
[c] Química Analítica, Y-TEC SA. Av. del Petróleo Argentino 900, Berisso, Buenos Aires, Argentina

ARTICLE INFO

Keywords:
Kaolin
Thermal behavior
Rare earth
Gadolinium oxide
Smart ceramic proppant

ABSTRACT

The effect of the addition of gadolinium oxide (Gd_2O_3) in the thermal behavior of a (66%) kaolinitic ball clay was studied and compared with the pure clay.

The incorporation of Gd_2O_3 is of technological interest for the design of smart ceramic proppants used for unconventional gas and oil well stimulation. This proppant material is used to obtain important information, such as the location and height of the created hydraulic fractures.

The studied comprised a set of thermal analysis up to 1400 °C and the sintering behavior of the clay, up to 5% addition. The developed texture and microstructure was also assessed.

No important effects in kaolinite dehydration temperature and mullites (primary and secondary) formation were observed (500–600 and 990 °C). The sintering range of the studied clay is 1080–1360 °C; the 5% wt. addition resulted in 80 °C decrease of the final sintering temperature.

Mixtures fired at 1250 and 1400 °C resulted in dense ceramic materials with mullite as principal crystalline phase accompanied by quartz and cristobalite; imbibed in a viscous glassy phase which was proportionally increased by the added oxide. The mullite content and cell parameters were not affected. No gadolinium containing binary or ternary crystalline phases were detected, inferring that the rare earth is dissolved by the active viscous glassy phase thermally formed from the clay crystalline phases.

Low concentration addition of the oxide did not affect the porosity or water absorption of the developed ceramics. Only the 5% wt. addition resulted in a slightly higher de-sinterization with the appearance of macroporosity if fired at 1400 °C.

1. Introduction

Ceramic proppants are frequently used in hydraulic fracturing of unconventional oil and gas reservoirs (Liang et al., 2016). Each hydraulic stimulation uses between 23 and 46 proppant tons and a well could use around 1.000 ton. The proppant specifications are ruled by the American Petroleum Institute (API) and its main requirements are: grain distribution size, sphericity, roundness, crush resistance, solubility, turbidity and hydraulic conductivity. Sintered proppants are developed to achieve fluid and gas conductivities under rigorous conditions of deep environments enables to support high temperatures, do not react with harsh chemical environments and deforms rather fracture under high stress.

After the well stimulation it is highly desirable to know the fracture morphology and proppants distribution.

Recently methods to identify proppants in induced formation fractures have been proposed have been proposed (US 8,129,318 B2, US Patent 8,234,072 B2, US 8,648,309 B2) and applied (Bhatia and Pande, 2016; Duenckel et al., 2011; Liu et al., 2015; Mulkern et al., 2010; Ortiz et al., 2016; Saldungaray et al., 2014; Torres et al., 2012; Velez et al., 2013). These methods require the incorporation of a suitable high thermal neutron capture compound, such as gadolinium, into the proppant grain during the ceramic manufacturing process. This is accomplished by incorporating a suitable high thermal neutron capture compound, such as gadolinium oxide, into each ceramic proppant grain during manufacturing process (US Patent 8,234,072 B2). Physical properties of the tagged proppant (e.g., crash strength and conductivity) are unaffected by the addition of Gd_2O_3 at a low concentration (0.025% to 1% by weight of the proppant) (US Patent 8,234,072 B2).

Ceramic proppants belong to the Al_2O_3-SiO_2 system and are manufactured from kaolin and/or bauxitic clays (US Patent 8,234,072 B2).

* Corresponding author at: Centro de Tecnología de Recursos Minerales y Cerámica (CETMIC): (CIC-CONICET-CCT La Plata), Camino Centenario y 506 s/n, C.C.49 (B1897ZCA), M.B. Gonnet, Argentina.
E-mail address: florenciahernandez@cetmic.unlp.edu.ar (M.F. Hernández).

http://dx.doi.org/10.1016/j.clay.2017.06.021
Received 17 March 2017; Received in revised form 21 June 2017; Accepted 22 June 2017
Available online 29 June 2017
0169-1317/

Hence, the thermal behaviors of kaolinitic clays mixtures with gadolinium oxide (Gd_2O_3) are of technological interest.

Gadolinium oxide (Gd_2O_3) adopts two crystalline structures cubic and monoclinic.

The cubic structure is similar to that of manganese (III) oxide. It features two types of gadolinium sites, each with a coordination number of 6 but with different coordination geometries. At room temperature the cubic phase is more stable. The phase change to the monoclinic structure takes place at 1200 °C.

Above 2100 °C to the melting point at 2420 °C, a hexagonal phase dominates. Rare earth silico-aluminate ternary glasses have been extensively studied for several applications (Kaewjang et al., 2014; Rocherulle et al., 1989). The principal application of Gd_2O_3 based materials arise from the magnetic and nuclear properties of gadolinium (Guo et al., 2004; Tsuzuki et al., 1999). The nuclear properties, involved in the mentioned proppants application, would not be affected by the typical ceramic thermal treatment.

In this work we describe the effect of gadolinium oxide addition to the thermal behavior of an industrial kaolinitic clay and evaluate the changes in the technological properties of the resulting ceramics. This will enlighten the processing strategy of gadolinium based ceramic proppants.

2. Experimental procedure

2.1. Materials

An industrial grade, secondary, kaolinitic ball clay was employed as the model clay (APM 112, Piedra Grande—La Toma SA, Neuquén, Argentina) (Cravero et al., 1997). The principal properties of the employed clay are shown in Table 1. A pure gadolinium oxide (Gd_2O_3) (Sigma Aldrich: CAS Number 12064-62-9) 99.9% pure was employed ($D_{50} \approx 2\,\mu m$).

2.2. Processing

The clay - oxide mixtures were obtained by wet ball milling; alumina jar and milling media were employed. Dried mixtures were disagglomerated and sieved (#200) before pressing. Disc (15 mm diameter) and prismatic (20.0 × 3.5 × 3.5 mm^3) shape samples were die pressed (100 MPa). The disc and prismatic shapes were chosen because they present more controllable dimension stability in comparison to the sphere morphology. The sphere proppants morphology can be obtained only through specific equipment like pelletizing disks or drums, or high energy mixers. The compaction obtained would be related to the conforming route and its particular processing variables.

Table 1
Chemical, mineralogical and grain size distribution of the Ball Clay; data taken from the commercial brochure.

Chemical composition	
Oxide	% wt.
SiO_2	57.0
Al_2O_3	27.5
Fe_2O_3	3.13
MgO	0.25
K_2O	0.85
Na_2O	0.13
TiO_2	0.15
CaO	0.18
Lost on ignition	5.3
Mineralogical composition	
Phase	% wt.
Kaolinite	66
Illite	9
Quartz	23
Feldspars	2
Particle size distribution evaluated by laser scattering	
Percentile	(μm)
D_{10}	0.11
D_{50}	2.03
D_{90}	11.01

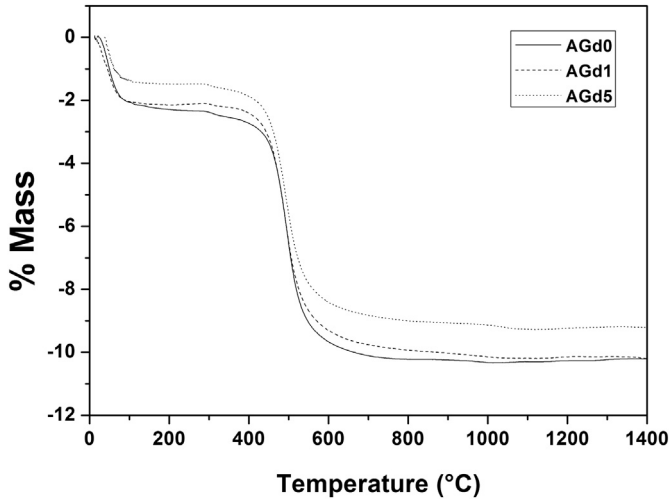

Fig. 1. Thermogravimetric analysis (TGA) of the studied clay and clay-Gd_2O_3 mixtures (0, 1 and 5% gadolinium oxide mixtures).

In our case the compaction grade was 55%. However the sintering behavior of ceramic based materials can be qualitatively extrapolate to different conformation routes. It is well known that the amount of mullite governs the mechanical properties of the clay based ceramic materials (Carty and Senapati, 1998; Serra et al., 2013), hence the disc and bar samples results might be extrapolated to sphere geometries.

Samples were fired at the same heating rate (10 °C/min) with different maximum temperatures at 1250 and 1400 °C and 30 min soaking in air atmosphere. In this study 1.0 and 5.0% wt. mixtures were studied and labeled AGd1 and AGd5. These were compared with the pure studied clay sample, labeled AGd0.

The lab scale geometries and press is a starting point to further compaction sintering study that could be carried out after this additive (Gd_2O_3) formulation study. This could be carried out with the incorporation of bauxite in order to optimize formulations more similar to the actually employed in the proppants industries. However the bauxite composition and the especially the accompanying minerals would make more difficult to establish the actual thermal reactions between the employed clay and rare earth oxide, that is being carried out in this study.

2.3. Characterizations

The effect of heat treatment was evaluated by thermogravimetric and differential thermal analysis (DTA-TG) simultaneously carried out on a Rigaku Evo II equipment with 10 °C/min as heating rate in Pt crucibles, in air atmosphere. The derivative curve of the TG (DTG) was also employed for this purpose. To understand the sintering behavior, thermo mechanical analysis on vertical prismatic (20.0 × 3.5 × 3.5 mm^3) sample was performed; with a 10 °C/min heating rate in air atmosphere (TMA Rigaku Evo plus II, Japan) (Rendtorff et al., 2016).

Afterwards, the linear shrinkage ($\Delta L/L_0$) was measured and the Archimedes immersion method was also carried out for calculating, apparent density and porosity of the fired samples. This three sintering parameters illustrate the actual sinterization grade of the resulting materials, ceramic proppants sinterization must be high in order to achieve high strength; the clay thermal shrinkage may be assumed to be

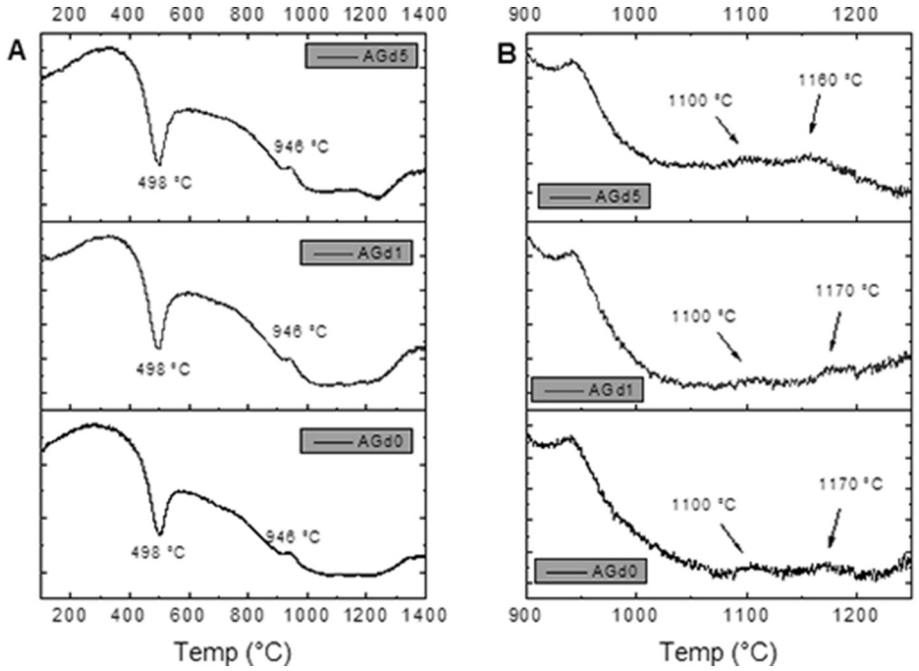

Fig. 2. Differential thermal analysis (DTA) of the studied clay and clay-Gd_2O_3 mixtures; right plot is a detail of the left one (0, 1 and 5% gadolinium oxide mixtures).

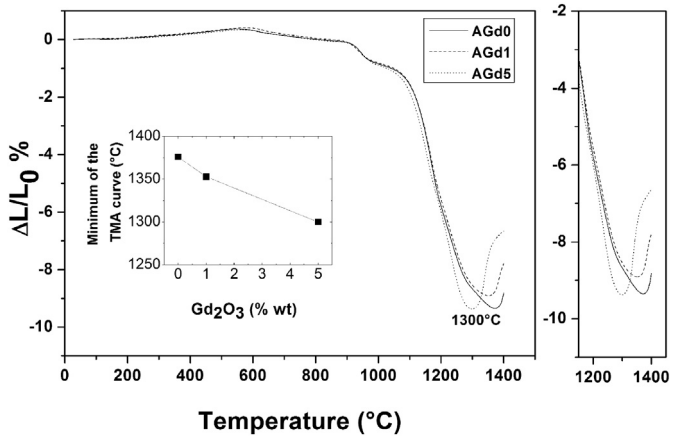

Fig. 3. TMA curves (dilatometry) of the clay and clay-Gd_2O_3 mixtures; right plot is a detail of the TMA curves. Scatter line inset plot presents minimum of the TMA curve as a function of the Gd_2O_3 content (0, 1 and 5% gadolinium oxide mixtures).

Table 2
Sintering parameters of the fired clay and clay-Gd_2O_3 mixtures.

Firing temperature	Sintering parameter	Gd_2O_3 content (wt%)		
		0	1	5
1250 °C	Liner shrinkage $\Delta L/L_0$ (%)	− 5.6	− 5.3	− 2.5
	Porosity (%)	20.0	27.0	32.0
	Density (g/cm^3)	1.98	1.73	1.72
1400 °C	Liner shrinkage $\Delta L/L_0$ (%)	− 0.4	1.6	2.9
	Porosity (%)	1.5	2.0	12.0
	Density (g/cm^3)	2.48	2.47	2.09

isotropic.

Identification and quantification of crystalline phases in the fired materials were carried out by X-ray diffraction (XRD) (Philips 3020 with Cu-Kα radiation, Ni filter, at 40 kV–35 mA; with 0.04° and 2 s steps in the 3–70° range). Phase identification from XRD patterns was carried out using PDF-2 database (ICDD PDF-2). Patterns were analyzed with the program FullProf (Version 5.40, March 2014) which is a multipurpose profile-fitting program (Rodríguez-Carvajal, 2001), including Rietveld refinement to perform phase quantification (Rietveld, 1969). The employed quantification method comprised both crystalline and non-crystalline phases. Particularly the amorphous glassy phase was quantified by the so called Le Bail method, in which this phase is introduced in the refinement as crystalline silica with extremely low crystallite size (Le Bail, 1995; Andrini et al., 2017; Conconi et al., 2014; Serra et al., 2013).

Finally the microstructure analysis was performed by a scanning electron microscope (SEM: JEOL, JCM-6000) (Fei Quanta 200). Gold coated polished (1.0 μm diamond paste) surface were analyzed in ultra-high vacuum conditions and 20.0 kV. An Everhart-Thornley Detector (ETD) was employed in back-scattered electron mode. Chemically etched (HF acid, 2 min) samples were also analyzed. Energy Dispersive Spectroscopy (EDS) analysis was carried out in mapping mode at 15 kV and 7800 s of acquisition time.

3. Results and discussions

3.1. Thermal analyses of the studied clay and Gd_2O_3 clay mixtures

The breakdown of clay minerals leading to the formation of amorphous or less crystalline components starts from about 500–600 °C with the formation of metakaolinite and finishes at around 1000 °C, giving rise to mullite and/or a viscous phase. This process continues with later abundant formation of vitreous phase, starting approximately from 1050 °C, whose composition apparently does not correspond to feldspar-quartz eutectics (feldspar melting is overwhelming quartz dissolution). Finally, a progressive dissolution of quartz in the vitreous phase, in absence of feldspars, takes place. Finished products, commonly fired at maximum temperature in the 1200–1350 °C range, contain essentially a vitreous phase associated with mullite, quartz and cristobalite (Carbajal et al., 2007; Gualtieri, 2007; Zanelli et al., 2011).

Generally all the complementary metals like potassium, sodium, calcium, magnesium, lithium, iron, titanium, etc. are dissolved in the viscous phase (Carty and Senapati, 1998; Zanelli et al., 2011).

Figs. 1–3 show the performed thermogravimetric analysis (TG), the differential thermal analyses (DTA) and the thermomechanical analyses (TMA) also known as dilatometry. In the present study no important

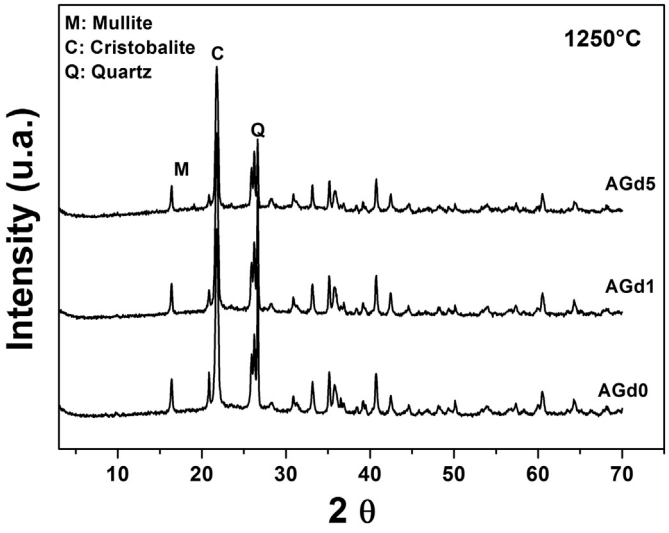

Fig. 4. XRD patterns of the clay and clay-Gd_2O_3 mixtures fired at 1250 °C. Reflections are labeled: M: Mullite, C: Cristobalite, Q: Quartz; the patterns have a vertical offset for better visualization.

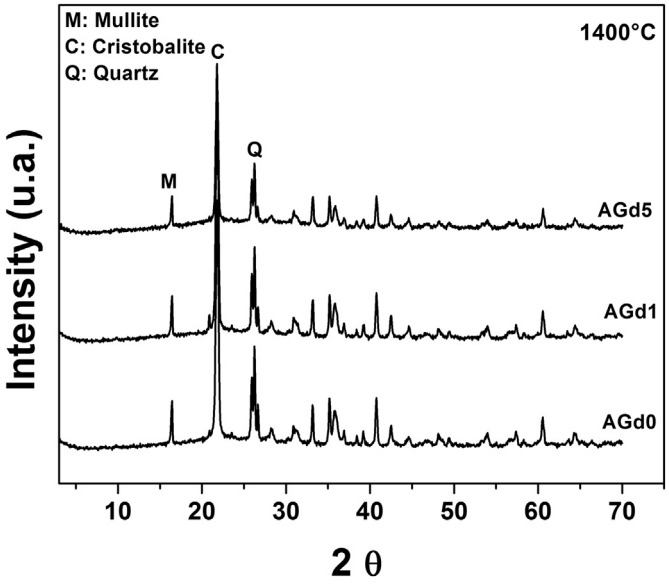

Fig. 5. XRD patterns of the clay and clay-Gd_2O_3 mixtures fired at 1400 °C. Reflections are labeled: M: Mullite, C: Cristobalite, Q: Quartz.

change in the gravimetric behavior was observed in the whole temperature range (room temperature to 1400 °C); the mass loss corresponding to surface water (50–110 °C) is equivalent for the three samples ≈ 2% wt. The chemical water mass loss (480–550 °C) follows the expected sequence (AGd0 > AGd1 > AGd5) and is coherent with the clay fraction content (Table 1).

The thermal behavior is similar to other kaolinitic clays (Bellotto et al., 1995a,b; Carbajal et al., 2007; Carty and Senapati, 1998; Chakraborty, 2014; De Aza et al., 2014; Gualtieri, 2007; Lee et al., 2008; MacKenzie et al., 1985; Okada et al., 1986; Ortega et al., 2010).

The differential thermal analysis revealed the same thermal processes with two endothermic peaks. At higher temperature (≈ 930 °C, centered at 946 °C) the spinel type aluminosilicate phase plus primary mullite formation process is evidenced by means of an exothermic and small peak; these processes were clearly not affected by the presence of the added rare earth oxide. Finally, secondary mullite formation, usually detected by a couple of exothermic small peaks in the 1100–1230 °C range (Okada et al., 1986; Schneider et al., 2008) were scarcely detected in the studied clay and clay oxide mixtures (Fig. 2, right plot). Particularly, position, shape and intensity of the peaks were not affected by the Gd_2O_3 addition.

The macroscopic thermal behavior of the clay and clay mixtures was recently fully described by Zanelli (Zanelli et al., 2011). The present studied materials revealed a similar behavior (Fig. 3). In this, the first thermal expansion (positive slope in the TMA) range can be observed, from room temperature to 500 °C. At this temperature an inflection can be observed and the samples start a minor shrinkage stage up to ≈ 950 °C, where an abrupt 1% sigmoidal shrinkage can be observed, that can be associated to the DTA spinel formation peak (Fig. 2). After this, a slight shrinkage stage can be observed that finishes at 1080 °C; at this temperature the viscous sintering of the ball clay starts (Zanelli et al., 2011). The shrinkage rate is constant around -5×10^{-4} °C^{-1} up to 1250 °C. From this temperature, the thermal behavior of the clay and the oxide mixtures slightly differs.

Fig. 3 shows the last range (1150–1400 °C) detail of the TMA; the slight difference between the three samples can be observed. The final sinterization temperature follows the AGd5 < AGd1 < AGd0 sequence. It was decreased linearly around 80 °C. The shrinkage is almost constant for the three samples. An over-firing is observed for the three samples, if fired at 1400 °C. But the expansion achieved during over firing is considerably higher for the AGd5 sample in comparison to the other two samples (almost 4% for AGd5 and around 1% for the AGd1 and AGd0).

3.2. Sintering parameters: shrinkage, apparent porosity and apparent density

The sintering parameters (Table 2) of the fired samples permit to observe the effect of the studied additive. The chosen clay sinter at 1400 °C, at 1250 °C 20% of porosity remains. After 1250 °C treatment the linear shrinkage ($\Delta L/L_0$) is 5.6%, and after 1400 °C the $\Delta L/L_0$ is almost null evidencing over-firing, and an evident expansion at the final stage of the firing processes. The achieved density at 1400 °C is high (2.48 g/cm^3), and at 1250 °C was around 2.0 g/cm^3.

The effect of the 1% Gd_2O_3 addition in the density was not important at 1400 °C; the lower density evaluated at 1250 °C and for the AGd5 sample evidence the presence of close porosity not evaluated by the Archimedes method, and perhaps over firing, corroborated by the positive value of $\Delta L/L_0$ achieved for AGd1 and AGd5 after the 1400 °C. The effect of 5% is more evident and shortens the sintering range, starting at the same temperature. This might be explained by the mineralogical thermal evolution of the clay oxide mixtures, shown in the next section.

This could be optimize if the firing program is changed to lower maximum temperatures, or by incorporating other mineralizer or secondary starting raw materials like feldspars, calcites, dolomites or talc. Further studies should be performed for the multiphase thermochemical processes of mentioned mixtures, but this falls out of the scope of this particular work.

3.3. XRD of the fired clay-Gd_2O_3 mixtures, Rietveld refinement and Le Bail method for glassy phase quantification

Figs. 4 and 5 show the XRD patterns of the studied materials. The typical amorphous band can be observed. The crystalline phases identified and quantified for the six samples were mullite ($3Al_2O_3.2SiO_2$), cristobalite (SiO_2) and quartz (SiO_2).

It is well known that the vast majority of the AI_2O_3-SiO_2-RE_2O_3 systems (RE: metal) are characterized by their glass-forming abilities (Kolitsch et al., 1997). The ternary system Al_2O_3-SiO_2-Gd_2O_3 was systematically studied by Kolitsch and Li groups (Kolitsch et al., 1997; Li et al., 1999). Several crystalline phases were identified and characterized. The glass forming zone is around the $3SiO_2{\cdot}Al_2O_3{\cdot}Gd_2O_3$ stoichiometry for 1300 and 1400 °C (Rocherulle et al., 1989); this were not observed in the evaluated XRD patterns.

Table 3
Crystalline phases and Rietveld refinement cell parameters of fired clay and 1–5% gadolinium oxide addiction.

Sample	AGd0		AGd1		AGd5	
Gadolinium oxide addition (wt. %)	0		1		5	
Firing temperature (°C)	1250	1400	1250	1400	1250	1400
R_{WP} (residual weight profile)	19.2	18.4	19.2	19.7	21.3	20.2
Quartz - PDF: 01-085-0797						
a (Å)	4.910(2)	4.9136(7)	4.910(2)	4.912(1)	4.9131(5)	4.891(3)
c (Å)	5.4002(7)	5.4025(1)	5.4023(3)	5.395(2)	5.4004(8)	5.431(6)
Mullite PDF: 00-015-0776						
a (Å)	7.553(4)	7.5574(4)	7.55(3)	7.558(4)	7.5548(6)	7.553(5)
b (Å)	7.7149(4)	7.7160(4)	7.7132(7)	7.7170(4)	7.7156(6)	7.7112(6)
c (Å)	2.8940(1)	2.8929(1)	2.8931(2)	2.8919(1)	2.8922(2)	2.8915(2)
Cristobalite 1 PDF: 01-082-0512						
a (Å)	5.019(5)	5.0228(4)	5.0179(3)	5.026(4)	5.0174(6)	5.018(6)
c (Å)	7.023(3)	6.9863(8)	6.998(3)	7.0092(8)	7.020(1)	6.997(1)
Cristobalite 2 PDF: 01-082-0512						
a (Å)	4.990(5)	4.9920(4)	4.993(4)	4.995(4)	4.9896(6)	4.997(7)
c (Å)	6.939(3)	6.9362(9)	6.934(4)	6.9558(9)	6.950(1)	6.951(1)

Table 4
Rietveld quantification (weight %) of the clay and clay-Gd_2O_3 mixtures.

Sample	Gd_2O_3 (wt. %)	Firing temperature (°C)	Phase	Mullite	Quartz	Cristobalite. 1	Cristobalite 2	Amorphous glassy phase (Le Bail method)
			Formula	$3Al_2O_3.2SiO_2$	SiO_2	SiO_2	SiO_2	Principally SiO_2
AGd0-1250	0	1250		37.0 (5)	9.6 (2)	15.5 (5)	10.7 (4)	27.2 (6)
AGd0-1400	0	1400		34.7 (7)	2.2 (1)	14.3 (6)	16.0 (7)	32.8 (6)
AGd1-1250	1	1250		36.5 (4)	9.1 (1)	12.6 (4)	12.6 (3)	29.2 (4)
AGd1-1400	1	1400		33.8 (5)	1.7 (1)	15.3 (3)	16.3 (4)	33.9 (6)
AGd5-1250	5	1250		33.5 (10)	5.4 (2)	11.7 (8)	12.4 (9)	37.1 (9)
AGd5-1400	5	1400		31.6 (7)	1.3 (2)	10.7 (5)	10.3 (6)	46.1 (9)

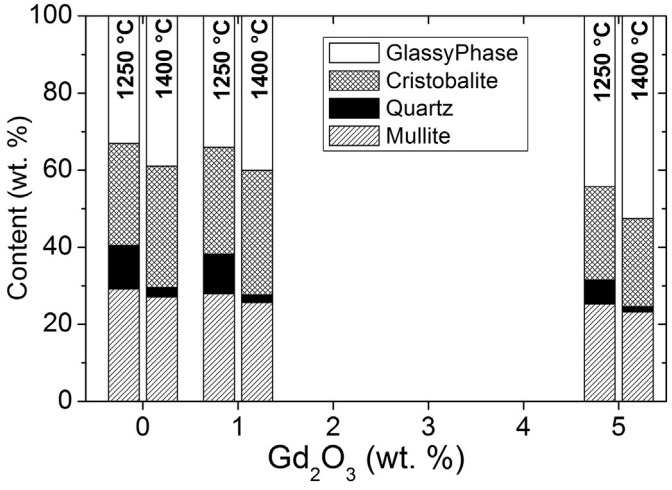

Fig. 6. Crystalline and glassy phase content as a function of gadolinium oxide addition of after firing (1250 and 1400 °C).

The results of the Rietveld refinement and PDF cards for each phase are shown and compared in Table 3. Table 4 summarizes the evaluated and quantified phases in each material. Global estimated standard deviations were derived from the estimated standard deviation on individual scale factors, for the respective phases, are presented in the table as well.

The shape of the cristobalite peaks could not be satisfactorily fitted by a lonely contribution. Two different cristobalite structures were proposed for the Rietveld refinement. This was previously proposed for similar materials, (Butler and Dyson, 1997; Madsen et al., 1991). Refined cell parameters for both cristobalites are shown in Table 3. This might be explained by the coexistence of two dissimilar phases. One produced from the kaolinite thermal decomposition and the other from the thermal transformation of the initial quartz present in the clay mineral, the second present minor impurities content.

The results of the quantifications together with Rwp residuals are shown in Table 3. The cell parameters of the crystalline phases as well. The Rwp values are adequate and similar to the ones achieved in similar materials (Andrini et al., 2016; Bonetto et al., 2003; Conconi et al., 2014; Hillier, 2000; Ruan and Ward, 2002; Serra et al., 2013; Serra et al., 2015). No gadolinium containing crystalline phases were detected. Besides the refined cell parameters of identified phases are in accordance with literature (Schneider et al., 2008), it can be stand that no important structural effect was observed after the addition of the rare earth oxide (Gd_2O_3).

In order to understand the effect of the rare earth addition in terms of the resulting phase proportions based on the Rietveld quantification, in Fig. 6 the phase contents are compared as a function of the added rare earth oxide for the two firing temperatures (1250 and 1400 °C). The stacked bar plot permits to observe that the mullite proportion slightly over the 20% wt., even after 1250 °C. It is well known that this phase governs the mechanical properties of the clay based ceramic materials (Carty and Senapati, 1998; Serra et al., 2013), and its proportion is slightly (nearly negligible) decreased by the Gd_2O_3 addition, in the studied range. This was observed in the DTA analysis as well. As a consequence the silica based phases: (quartz, cristobalite and glassy phases) total proportion is not affected by the studied addition. The quartz proportion after 1250 °C was around 10% for AGd0 and AGd1, but for AGd5 it is around 6 wt. %, showing that the oxide addition enhanced the quartz-cristobalite thermal transformation. After 1400 °C

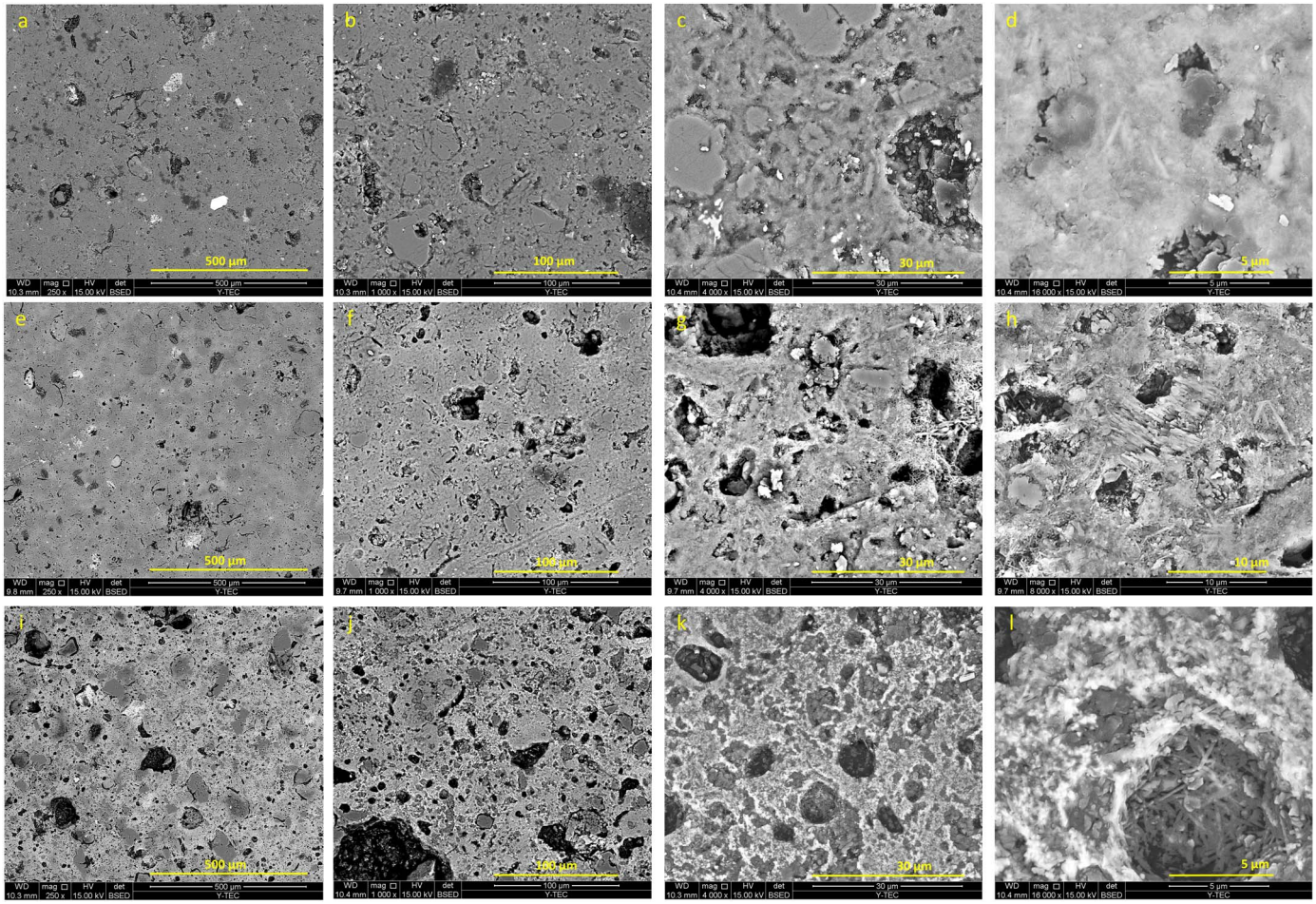

Fig. 7. a–l: SEM images of the clay and clay-Gd_2O_3 mixtures fired at1400 °C (AGd0 a–d; AGd1 e–h; AGd5 i–l) respectively (from left to right: 250 ×, 1000 ×, 4000 × and 16,000 ×).

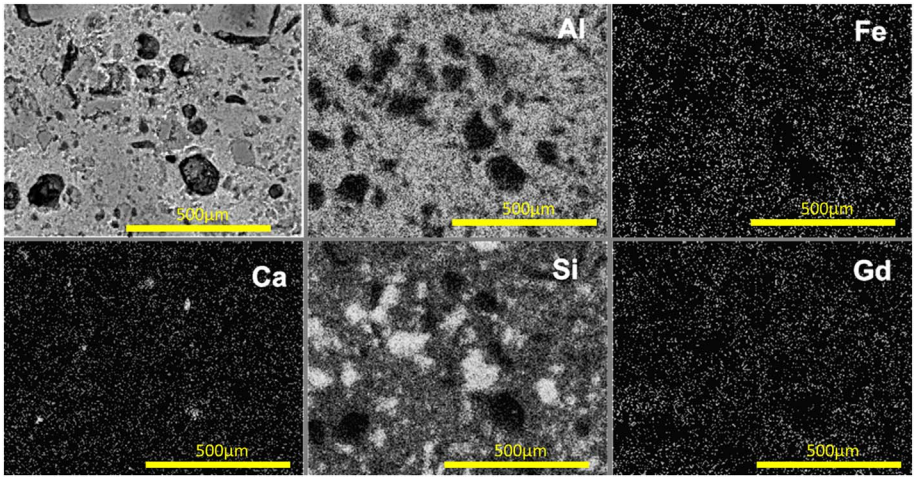

Fig. 8. AGd5 × 4000 SEM image and the corresponding EDS mapping. 2D distribution of aluminum, iron, calcium, silicon and gadolinium atoms (Al, Fe, Ca, Si and Gd respectively).

the amount of quartz is low in the three studied samples. A noticeable effect of the Gd_2O_3 can be observed in the cristobalite - glassy phase relation. The amount of glassy phase is enhanced by the presence of the rare earth oxide in the whole studied range. If the rare earth results to be dissolved by the glassy phase, as it is concluded, the particular gadolinium oxide proportion in the glassy phase would be around 10 wt. %.

3.4. Microstructure analysis of the clay and clay-Gd_2O_3 mixtures fired a 1400 °C by scanning electron microscope

The developed microstructures was evaluated by means of scanning electron microscopy, the dense and complex microstructure of the ceramic is revealed (Fig. 7a–l). Pore (in black), can be identified in the matrix (different grays). The matrix can be described as a complex microstructure of crystalline grains (several microns) imbibed in the glassy (amorphous-viscous) continuous phase. Grains correspond to the crystalline phases detected by XRD: mullite, quartz and cristobalite. The glassy majorly silica based phase was also observed. Pore amount

follows the AGd0 < AGd1 < AGd5 sequence, as evaluated by the Archimedes method. Rounded macro-pores (≈ 100 μm) are complemented by a micro (meso) porosity only observed in greater magnifications. The observed microstructures are equivalent to the microstructures extensively reported in literature (Chakraborty, 2014; Iqbal and Lee, 2000; Lee et al., 2008).

In general the microstructures of the ceramics were not importantly affected by the addition of the rare earth oxide. The amount of the macro-pores was increased by the addition of Gd_2O_3. This is an evidence of the over sinterization or over firing of the material, showing that the maturation range was decreased by the addition, previously observed by TMA (Fig. 3). This fact might be related to the higher amount of glassy phase quantified by XRD. Particularly, Fig. 7d, h and l clearly show the acicular mullite grains in the three samples; this was observed by XRD (Figs. 3 and 4).

A simple EDS analysis was carried out in order to corroborate the gadolinium presence. The evaluated amounts of Gd element were 0.0, 0.7 and 3.2% wt. in the AGd0-AGd1-AGd5 series. This, within the typical EDS error corresponds to the incorporated oxide, evidencing the lack of loss of rare earth element during thermal treatments.

Finally the elemental mapping was performed for the 5% Gd_2O_3 added sample (AGd5) fired at 1400 °C with 4000 enlargements for the principal elements: Al, Si, Fe, Ca and Gd. (Fig. 8). The silicon distribution is heterogeneous, pores (in black) and higher concentration of this element correspondingly to cristobalite or quartz grains can be easily devised. The aluminum distribution is relatively homogeneous, this corresponds to mullite ($3Al_2O_3{\cdot}2SiO_2$); in this case, the pores and cristobalite can be observed in black. Calcium and Iron distribution give not important information. Finally the gadolinium distribution is clearly homogeneous in the developed microstructure; presumably distributed in the viscous glassy silica based matrix where the other phases are imbibed.

4. Conclusions

The effect of a rare earth oxide (Gd_2O_3) addition in the thermal behavior of kaolinitic (66% wt.) ball clay and the technological properties of the resulting ceramics if fired at 1250 and 1400 °C was performed. A systematic formulation-sintering-properties correlation was carried out.

The thermo-chemical complex processes were not affected by the presence of the Gd_2O_3. Particularly no important effect in the temperature of the kaolinite dehydration and mullite, formation were observed (450–600 and 990 °C). The sintering temperature range of the studied clay is 1080–1360 °C; the 5% wt. oxide addition resulted in 80 °C decrease of the final sintering temperature. The 1% addition did not affect the thermochemical behavior of the clay.

Like the model clay, mixtures fired at 1250 and 1400 °C resulted in relatively dense ceramic materials with mullite as principal crystalline phases accompanied by quartz and cristobalite, imbibed in a viscous glassy phase which was proportionally increased by the added oxide. Mullite cell parameters were not affected. No gadolinium containing binary or ternary crystalline phases were detected, inferring that the rare earth is dissolved by the active viscous glassy phase thermally formed from the clay crystalline phases.

Low concentration addition of the oxide did not affect the porosity or water absorption of the developed ceramics. Only the 5% wt. addition resulted in a slightly higher de-sinterization with the appearance of macro-porosity if fired at 1400 °C.

Finally, it can be concluded that the incorporation of this oxide to the possible formulation of a ceramic proppants would not imply important changes in the processing route.

Acknowledgments

This work has been partially supported by Nano-Petro FONARSEC Project 2012 (ANPCyT). MFH acknowledge CONICET and Y-Tec for the fellowship. The authors want to express their gratitude to M. Bernarda Epele and Alejandra Floridia for the help in the SEM analysis.

References

Andrini, L., Gauna, M.R., Conconi, M.S., Suarez, G., Requejo, F.G., Aglietti, E.F., Rendtorff, N.M., 2016. Extended and local structural description of a kaolinitic clay, its fired ceramics and intermediates: an XRD and XANES analysis. Appl. Clay Sci. 124, 39–45.

Andrini, L., Moreira Toja, R., Gauna, M.R., Conconi, M.S., Requejo, F.G., Rendtorff, N.M., 2017. Extended and local structural characterization of a natural and 800 °C fired Na-montmorillonite–patagonian bentonite by XRD and Al/Si XANES. Appl. Clay Sci. 137, 233–240.

Bellotto, M., Gualtieri, A., Artioli, G., Clark, S.-M., 1995a. Kinetic study of the kaolinite-mullite reaction sequence. Part I: Kaolinite dehydroxylation. Phys. Chem. Miner. 22, 207–214.

Bellotto, M., Gualtieri, A., Artioli, G., Clark, S.-M., 1995b. Kinetic study of the kaolinite-mullite reaction sequence. Part II: Mullite formation. Phys. Chem. Miner. 22, 215–222.

Bhatia, K., Pande, K., 2016. First Application of Nonradioactive Tracer Technology in CSG Unconventional Basin in Central India: Optimization and Evaluation of Fracturing Treatment. Society of Petroleum Engineers. https://doi.org/10.2118/181782-MS SPE-181782-MS.

Bonetto, R.D., Zalba, P.E., Conconi, M.S., Manassero, M., 2003. The Rietveld method applied to quantitative phase analysis of minerals containing disordered structures. Rev. Geol. Chile 30, 103–115.

Butler, M.A., Dyson, D.J., 1997. The quantification of different forms of cristobalite in devitrified alumino-silicate ceramic fibres. J. Appl. Crystallogr. 30, 467–475.

Carbajal, L., Rubio-Marcos, F., Bengochea, M.A., Fernandez, J.F., 2007. Properties related phase evolution in porcelain ceramics. J. Eur. Ceram. Soc. 27, 4065–4069.

Carty, W.M., Senapati, U., 1998. Porcelain-raw materials, processing, phase evolution and mechanical behaviour. J. Am. Ceram. Soc. 81, 3–20.

Chakraborty, A.K., 2014. Phase Transformation of Kaolinite Clay. Springer, New Delhi.

Conconi, M.S., Gauna, M.R., Serra, M.F., Suarez, G., Aglietti, E.F., Rendtorff, N.M., 2014. Quantitative firing transformations of a triaxial ceramic by X-ray diffraction methods. Cerâmica 60, 524–531.

Cravero, F., Gonzalez, I., Galan, E., Dominguez, E., 1997. Geology, mineralogy, origin and possible applications of some Argentinian kaolins in the Neuquen basin. Appl. Clay Sci. 12, 27–42.

De Aza, A.H., Turrillas, X., Rodriguez, M.A., Duran, T., Pena, P., 2014. Time-resolved powder neutron diffraction study of the phase transformation sequence of kaolinite to mullite. J. Eur. Ceram. Soc. 34, 1409–1421.

Duenckel, R.J., Smith, H., Warren, W.A., Grae, A.D., 2011. Field application of a new proppant detection technology. In: SPE International. SPE 146744.

Gualtieri, A.F., 2007. Thermal behavior of the raw materials forming porcelain stoneware mixtures by combined optical and in situ X-ray dilatometry. J. Am. Ceram. Soc. 90, 1222–1231.

Guo, H., Yang, X., Xiao, T., Zhang, W., Lou, L., Mugnier, J., 2004. Structure and optical properties of sol–gel derived Gd2O3 waveguide films. Appl. Clay Sci. 230, 215–221.

Hillier, S., 2000. Accurate quantitative analysis of clay and other minerals in sandstones by XRD: comparison of a Rietveld and a reference intensity ratio (RIR) method and the importance of sample preparation. Clay Miner. 35, 291–302.

Iqbal, Y., Lee, W.E., 2000. Microstructural evolution in triaxial porcelain. J. Am. Ceram. Soc. 83, 3121–3127.

Kaewjang, S., Maghanemi, U., Kothan, S., Kim, H.J., Limkitjaroenporn, P., Kaewkhao, J., 2014. New gadolinium based glasses for gamma-rays shielding materials. Nucl. Eng. Des. 280, 21–26.

Kolitsch, U., Seifert, H.J., Aldinger, F., 1997. Phase relationships in the system Gd_2O_3-Al_2O_3-SiO_2. J. Alloys Compd. 257, 104–114.

Le Bail, A., 1995. Modelling the silica glass structure by the Rietveld method. J. Non-Cryst. Solids 183, 39–42.

Lee, W.E., Sarvornpanich, T., Iqbal, Y., 2008. Mullite formation in clays and clay-derived vitreous ceramics. J. Eur. Ceram. Soc. 28, 465–471.

Li, L., Tang, Z., Sun, W., Wang, P., 1999. Phase diagram estimation of the Al_2O_3–SiO_2–Gd_2O_3 system. Phys. Chem. Glasses 40, 126–129.

Liang, F., Sayed, M., Al-Muntasheri, A.G., Chang, F.F., Li, Leiming, 2016. A comprehensive review on proppant technologies. Petroleum 2, 26–39.

Liu, J., Zhang, F., Gardner, R.P., Hou, G., Zhang, Q., Li, H., 2015. A method to evaluate hydraulic fracture using proppant detection. Appl. Radiat. Isot. 105, 139–143.

MacKenzie, K.J.D., Brown, I.W.M., Meinhold, R.H., Bowden, M.E., 1985. Outstanding problems in the kaolinite-mullite reaction sequence investigated by 29Si and 27Al solid-state nuclear magnetic resonance: I, metakaolinite. J. Am. Ceram. Soc. 68, 293–297.

Madsen, I.C., Finney, R.J., Flann, R.C.A., Frost, M.T., Wilson, B.W., 1991. Quantitative analysis of high-alumina refractories using X-ray powder diffraction data and the Rietveld method. J. Am. Ceram. Soc. 74, 619–624.

Mulkern, M., Masnyk, B., Kramer, H., Sites, J., 2010. A green alternative for determination of frac height and proppant distribution. In: SPE International. SPE 138500.

Okada, K., Otsuka, N., Ossaka, J., 1986. Characterization of spinel phase formed in the kaolin-mullite thermal sequence. J. Am. Ceram. Soc. 69, C251–C253.

Ortega, A., Macías, M., Gotor, F.J., 2010. The multistep nature of the kaolinite dehydroxylation: kinetics and mechanism. J. Am. Ceram. Soc. 93, 197–203.

Ortiz, A.C., Hry, D.E., Martínez, J.R., Varela, R.A., 2016, February. Hydraulic Fracture

Height Estimation in an Unconventional Vertical Well in the Vaca Muerta Formation, Neuquen Basin, Argentina. Society of Petroleum Engineers SPE-179145-MS.
Rendtorff, N.M., Gómez, S., Gauna, M.R., Conconi, M.S., Suarez, G., Aglietti, E.F., 2016. Dense mullite–zirconia–zirconium titanate ceramic composites by reaction sintering. Ceram. Int. 42, 1563–1572.
Rietveld, H., 1969. A profile refinement method for nuclear and magnetic structures. J. Appl. Crystallogr. 2, 65–71.
Rocherulle, J., Verdier, P., Laurent, Y., 1989. Preparation and properties of gadolinium oxide and oxynitride glasses. Mater. Sci. Eng. B 2, 265–268.
Rodríguez-Carvajal, J., 2001. Recent developments of the program FULLPROF, in commission on powder diffraction (IUCr). Newsletter 26, 12–19.
Ruan, C.D., Ward, C.R., 2002. Quantitative X-ray powder diffraction analysis of clay minerals in Australian coals using Rietveld methods. Appl. Clay Sci. 21, 227–240.
Saldungaray, P., Duenckel, R.J., Palisch, T.T., 2014, September. Reducing Hydraulic Fracturing HSE Footprint through the Application of a Non-Radioactive Method for Proppant Placement and Propped Fracture Height Assessment. InSPE Middle East Health, Safety. Society of Petroleum Engineers SPE-170333-MS.
Schneider, H., Schreuer, J., Hildmann, B., 2008. Structure and properties of mullite. A review. J. Eur. Ceram. Soc. 28, 329–344.
Serra, M.F., Conconi, M.S., Suarez, G., Agietti, E.F., Rendtorff, N.M., 2013. Firing transformations of an argentinean calcareous commercial clay. Cerâmica 59, 254–261.
Serra, M.F., Conconi, M.S., Suarez, G., Aglietti, E.F., Rendtorff, N.M., 2015. Volcanic ash as flux in clay based triaxial ceramic materials, effect of the firing temperature in phases and mechanical properties. Ceram. Int. 41, 6169–6177.
Torres, F., Reinoso, W., Tierra, Gran, Chapman, M., Han, X., Carbo, Ceramics, Campo, P., Halliburton, 2012. Field aplication of a new proppant-detection technology- a case history in the Putumayo basin of Colombia. In: SPE International. SPE 152251.
Tsuzuki, T., Pirault, E., McCormick, P.G., 1999. Mechanochemical synthesis of gadolinium oxide nanoparticles. Nanostruct. Mater. 11, 125–131.
Velez, E.I., Ponce, J.E., Tessari, S., 2013. Determining Hydraulic-Fracture Orientation and Height Using After-Fracture Borehole Acoustic Attributes in the Vaca Muerta Unconventional Reservoirs. Society of Petroleum Engineers SPE-166421-MS.
Zanelli, C., Raimondo, M., Guarini, G., Dondi, M., 2011. The vitreous phase of porcelain stoneware: composition, evolution during sintering and physical properties. J. Non-Cryst. Solids 357, 3251–3260.